17
Nanofluidics

Nanofluidics is an emerging research field, which deals with fluid flow on the nanometer scale. It is being boosted by the ongoing development of nanotechnological tools and techniques, and it contains the potential for both basic research, e.g. an improved understanding of the limitations and ultimate breakdown of the classical continuum description of fluid dynamics for spatially confined liquids, as well as for technology, e.g. the development of devices for handling of single molecules in solution. In this chapter we shall study a few selected topics within nanofluidics.

17.1 Investigation of the no-slip boundary condition

Since its introduction in Eq. (3.1) we have in this book applied the no-slip boundary condition $\mathbf{v} = \mathbf{v}_{\text{wall}}$ for liquids at the boundary of a solid wall moving with velocity $\mathbf{v}_{\text{wall}}$. This boundary condition is well tested regarding liquid flow on the macroscale, but in the following we shall look into some of the experimental evidence for its validity in micro- and nanofluidics. Thanks to the development of new experimental techniques within the past decade, the no-slip hypothesis has been questioned in a number of experimental studies on the micro- and nanometer scale. While minor deviations from the no-slip boundary conditions have only negligible effects on macroscale liquid flow behavior, they could be of significance in micro- and nanofluidic systems.

We consider the infinite parallel-plate channel of Section 3.4.2 with stationary walls and a flow velocity parallel to the x axis, $\mathbf{v} = v_x(z)\,\mathbf{e}_x$. Already in the nineteenth century Navier discussed a more general boundary condition than no-slip $v_x(0) = 0$ at the bottom plate situated at $z = 0$. This so-called Navier boundary condition reads

$$v_x(0) = \lambda_s\, \partial_z v_x(0), \quad \text{(wall at } z = 0\text{)}, \tag{17.1}$$

where λ_s is the slip length or Navier length defined as the distance behind the boundary where the tangent of the velocity field intersects the x axis. Note that for $\lambda_s = 0$ we recover the usual no-slip boundary condition. A geometrical interpretation of the Navier boundary condition and the slip length λ_s is shown in Fig. 17.1(a). In the case of a general surface at rest with an outward pointing normal vector $\mathbf{n}$, see Fig. 2.1, the Navier boundary condition for the normal component $\mathbf{v}_n = (\mathbf{n}\cdot\mathbf{v})\mathbf{n}$ and the tangential component $\mathbf{v}_t = \mathbf{v} - (\mathbf{n}\cdot\mathbf{v})\mathbf{n}$ is

$$\mathbf{v}_n = \mathbf{0}, \tag{17.2a}$$

$$\mathbf{v}_t = -\lambda_s(\mathbf{n}\cdot\boldsymbol{\nabla})\mathbf{v}_t. \tag{17.2b}$$

Joseph and Tabeling (2005) have reported a careful measurement of the velocity profile of deionized water flowing in a 100 μm wide and 10 μm high microchannel with a transparent

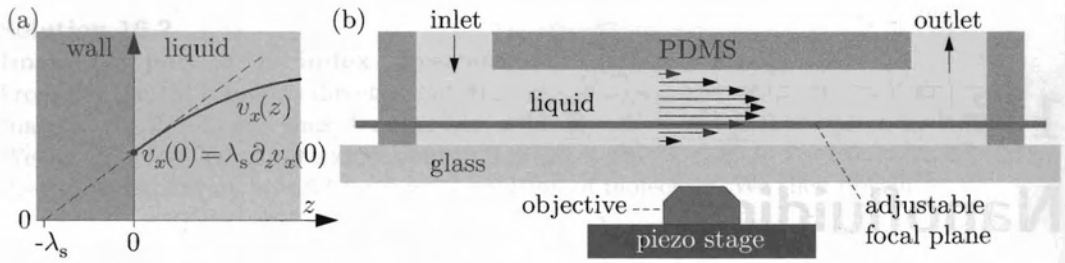

Fig. 17.1 (a) The Navier boundary condition $v_x(0) = \lambda_s\, \partial_z v_x(0)$, where the slip length λ_s is defined as the intersect of the slope of the velocity profile at the wall and the z axis. (b) Sketch of the experimental setup used by Joseph and Tabeling (2005) to measure the slip length in a microfluidic channel of height 10 μm. The velocity profile was scanned by adjusting the position of the focal plane with the piezo-stage carrying the microscope objective. For each position of the focal plane the velocity was measured using microparticle-image velocimetry.

glass bottom wall and the polymer PDMS for the other walls, see the sketch in Fig. 17.1(b). By using an objective with a large numerical aperture (NA = 1.3) they obtained a well-defined depth of field of 700 nm, and as the objective was mounted on a piezo-stage, they could move the focal plane in vertical steps of 50 nm up through the microchannel. The flow velocity was measured by particle-image velocimetry (PIV) on fluorescent tracer particles of radius $a = 50$ nm dissolved in the water in a volumetric concentration of 10^{-5}, i.e. small enough to give a good spatial resolution and large enough to suppress their Brownian motion. Each PIV recording involved a volume of size $25 \times 12 \times 0.5\ \mu\text{m}^3$.

Some of their results are shown in Fig. 17.2. In panel (a) it is seen how well their data points for the velocity fall on top of a Poiseuille parabola. Deviations are seen close to the bottom wall situated at $z = 2$ μm, but these are explained by Debye-layer effects due to the different zeta-potentials of the tracer particles and the bottom wall. In panel (b) is seen a summary of several determinations of the slip length λ_s for different values of the shear rate $\partial_z v_x$ at the bottom wall. Joseph and Tabeling concluded this part of their measurements by stating the following slip length for water on glass:

$$\lambda_s = 50\ \text{nm} \pm 50\ \text{nm}, \quad \text{for water on glass.} \tag{17.3}$$

Their results do not invalidate the no-slip hypothesis, but on the other hand it is possible that a non-zero slip length less than 100 nm in fact does exist.

Let us analyze how a slip length $\lambda_s = 50$ nm would affect the hydraulic resistance $R_{\text{hyd}}(\lambda_s)$ of microchannel in comparison with the no-slip resistance $R_{\text{hyd}}(0)$. We consider a pressure-driven flow in an infinite parallel-plate channel of height h given a Navier boundary condition with a non-zero slip length λ_s on both bottom and top plates. Due to symmetry the problem is easier solved when placing the bottom plate at $\tilde{z} = -h/2$ and the top plate at $\tilde{z} = h/2$, instead of the usual $z = 0$ and $z = h$ positions. We denote the length, width, pressure drop and viscosity by L, w, Δp and η, respectively. As shown in Exercise 17.1 the velocity field $v_x(\tilde{z})$ becomes

$$v_x(\tilde{z}) = \frac{\Delta p}{2\eta L}\left[\left(1 + 4\frac{\lambda_s}{h}\right)\left(\frac{h}{2}\right)^2 - \tilde{z}^2\right], \tag{17.4}$$

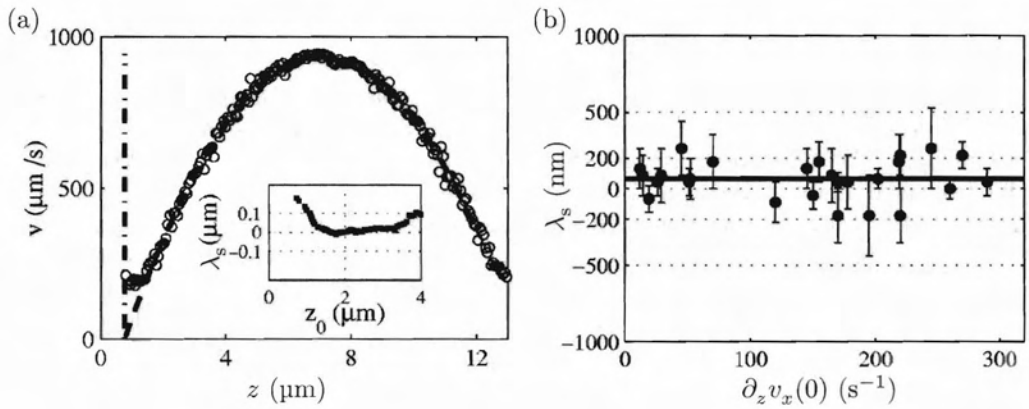

Fig. 17.2 Measurements of the velocity profile of deionized water in a 100 μm wide and 10 μm high microchannel. (a) Particle-image velocimetry measurements (open circles) of the velocity $v_x(z)$ as a function of the position z of the focal plane. The vertical dash-dotted line represents the position of the bottom glass plate of the microchannel. The dashed line, mostly covered by the data points, is the best fit to a parabola. The data points deviate from the parabola close to the bottom wall due to electrical effects stemming from the different zeta-potentials of the tracer particles and the wall, see Section 8.3. The inset shows the value obtained for the slip length λ_s as a function of left cutoff of the data points. Data points more than 1 μm away from the bottom wall leads to the same slip length. (b) The slip length λ_s measured for different values of the shear rate $\partial_z v_x(0)$ at the bottom wall. The overall result is $\lambda_s = 50$ nm $\pm$ 50 nm. Figures reprinted by permission from P. Joseph and P. Tabeling, Phys. Rev. E **71**, 035303(R) (2005). Copyright (2005) by the American Physical Society.

from which we recover the usual no-slip solution when $\lambda_s = 0$.

The explicit velocity field in Eq. (17.4) is easily integrated to yield the flow rate $Q(\lambda_s)$, from which the hydraulic resistance $R_{hyd}(\lambda_s)$ is readily deduced, again see Exercise 17.1,

$$R_{hyd}(\lambda_s) = \frac{1}{1+6\frac{\lambda_s}{h}}\,\frac{12\eta L}{h^3 w} = \frac{R_{hyd}(0)}{1+6\frac{\lambda_s}{h}}. \tag{17.5}$$

This expression reveals that if it were possible to increase the slip length to infinity, the hydraulic resistance, and thus viscous dissipation of energy, would vanish, which is indeed, an interesting perspective. However, even the small slip length $\lambda_s = 50$ nm influences the hydraulic resistance significantly for channels of small height. For $h = 10$ μm we get $R_{hyd}(\lambda_s) = 0.97\, R_{hyd}(0)$, a reduction of 3%, while for $h = 1$ μm we get $R_{hyd}(\lambda_s) = 0.77\, R_{hyd}(0)$, a significant reduction of 23%.

In the literature are found reports of λ_s in the micrometer range, e.g. Tretheway and Meinhart (2002). Such extreme slip lengths, although desirable to achieve, are not very robust, probably because layers of gas forming between the liquid and the wall seem to be involved. It is fair to state that the last word has not yet been said about non-zero slip lengths for liquids flowing in micro- and nanofluidic systems.

17.2 Capillary filling of nanochannels

Using state-of-the-art nanotechnology it is possible to fabricate fluid channels having cross-sections of linear sizes in the nanometer range. In the literature, applications of such nanofluidic channels have been reported within studies of fundamental physical properties, Kameoka and Craighead (2001), van der Heyden, Stein, and Dekker (2005), Tas *et al.* (2004), as well as bio/chemical analysis, Bakajin (1998) and Reisner *et al.* (2007).

We use the work presented by Anders Kristensen's group at MIC-DTU on capillary filling of nanochannels as an example of fluidics in flat, straight channels with rectangular cross-sections of heights less than 1 μm, see Persson *et al.* (2007). In Fig. 17.3 is shown a top view of the channel design and the principle of the fabrication method that leads to a control on the nanometer scale of the channel height. The nanofluidic properties are investigated by using the channel as a capillary pump, see Section 7.4.1. Pure (milli-Q) water or a 0.1 M NaCl electrolyte is loaded into the large micrometer-sized inlet channel, from where the liquid is sucked into the connected nanochannels by the capillary force. The advancement of the position $L(t)$ at time t of the front meniscus is recorded by a video camera attached to an optical microscope. The width of the channels is $w = 10$ μm, while the heights are less than 1 μm making the aspect ratio h/w less than 0.01. Neglecting the small aspect ratio correction, the expression Eq. (7.36) for the square $L^2(t)$ of the meniscus position becomes

$$L^2(t) = \frac{h\gamma \cos\theta}{3\eta}\, t \equiv a_{\mathrm{p}}\, t, \tag{17.6}$$

where $\cos\theta = \frac{1}{2}\big(\cos\theta_1 + \cos\theta_2\big)$ is the average between the cosine of the contact angle of the SiO_2 bottom wall and glass top lid, see Exercise 7.3, and where we have introduced the slope a_{p} for the expected linear dependence of L^2 versus time t for a Poiseuille flow profile. At 25 °C the experimental parameter values are $\eta = 0.89$ mPa s, $\gamma = 73$ mJ/m^3, and $\cos\theta = 0.96$, which results in the following dependence of channel height h for the expected slope a_{p}, based on Poiseuille flow,

$$a_{\mathrm{p}} = h \times 26 \text{ m/s}. \tag{17.7}$$

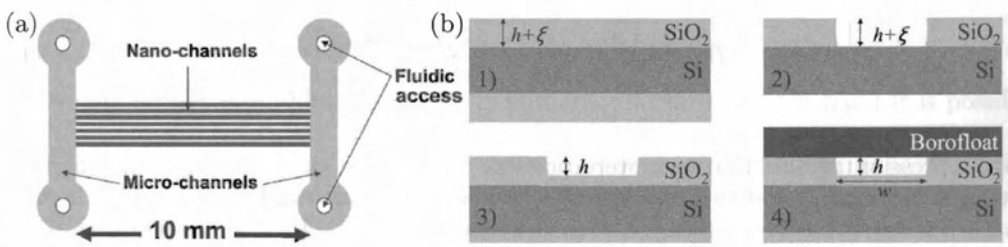

Fig. 17.3 (a) Top view of a chip containing seven nanochannels (dark gray) of length $L = 10$ mm, width $w = 10$ μm, and height h ranging from 14 to 300 nm. The nannochannels connect two microchannels (light gray) furbished with access ports through which liquid is introduced into the system. (b) The fundamental steps in the fabrication process: 1) First oxidation. 2) Wet isotropic BHF etch through an etch mask resulting in slightly sloped sidewalls. 3) Second oxidation, which is faster inside the channel region, where the oxide layer is thinner, than outside. 4) Bonding of glass lid. Adapted from Persson *et al.* (2007) courtesy of Anders Kristensen, MIC-DTU.

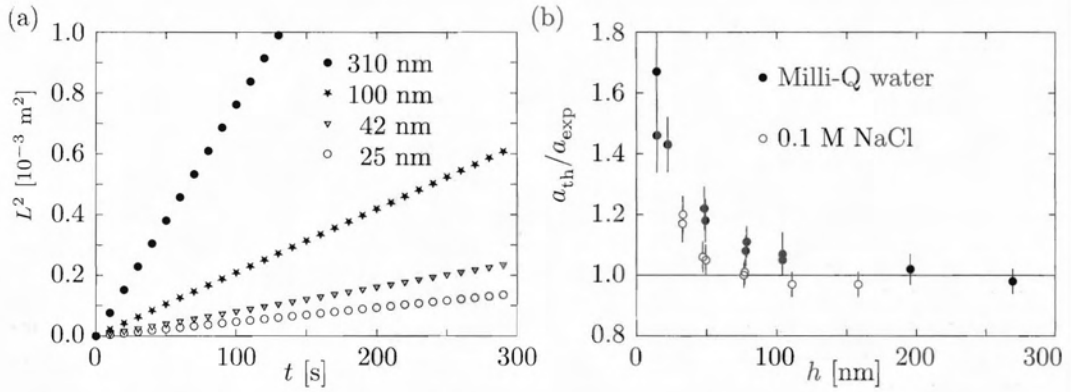

Fig. 17.4 (a) Measurements of the linear relationship $L^2 = a\,t$ between the square of the meniscus position L and time t for channel heights $h = 25$, 42, 100, and 310 nm. (b) The ratio a_p/a_{exp} of the theoretical Poiseuille-flow slope a_p and the experimental slope a_{exp} for the capillary filling $L^2(t) = a\,t$ for the nanochannel. The filling liquids are Milli-Q water and an 0.1 M NaCl aqueous solution. Every data point is an averaged value from between 20 and 50 measurements. The channel width is $w = 10$ μm. Adapted from Persson *et al.* (2007) courtesy of Fredrik Persson, MIC-DTU.

In Fig. 17.4 are shown some of the experimental results. Panel (a) is a scanning electron microscope picture of an actual nanochannel of height $h = 75$ nm and width $w = 10$ μm, while panel (b) contains graphs of $L(t)^2$ for four small channel heights h, as well as a plot of the ratio a_{exp}/a_p as a function of channel height h between experimentally measured and theoretically expected slopes a_{exp} and a_p, respectively. The data exhibits two very clear features: First, the square L^2 of the meniscus position depends indeed linearly on time t, and secondly, while the measured slopes a_{exp} of the obtained straight lines agree well with the theoretically expected slope a_p for large channel heights, a significant and systematically increasing deviation is observed as the channel heights are decreased below approximately 100 nm.

Traditionally, the deviation of the measured slope from the slope expected from Poiseuille flow is expressed as the ratio a_p over a_{exp}. This emphasizes the observation of a relative increase in the resistance against capillary flow. As $a_p \propto 1/\eta$ this increase can be summarized by introducing either a phenomenological effective viscosity η_{eff}, the hydraulic resistance ratio $R^{exp}_{hyd}/R^{p}_{hyd}$, or the flow rate ratio Q_p/Q_{exp}, where the indices "exp" and "p" refer quantities measured for the actual flow or expected for a pure Poiseuille flow, respectively, in the same nanochannel with a given Young–Laplace pressure drop Δp_{surf},

$$\frac{a_p}{a_{exp}} = \frac{\eta_{eff}}{\eta} = \frac{R^{exp}_{hyd}}{R^{p}_{hyd}} = \frac{Q_p}{Q_{exp}}. \tag{17.8}$$

If the experimental flow is a pure Poiseuille flow we expect a height-independent ratio $a_p/a_{exp} = 1$, but clearly the ratio is not constant so we must look for additional contributions to the flow. In the following, we first investigate the possible influence from electro-osmosis and then from a non-zero slip length.

Both pure water and 0.1 M NaCl are electrolytes, so as described in Section 8.3, the introduction of these liquids into the nanochannels leads to the formation of Debye-layers

of thickness λ_D in the liquid adjacent to the channel walls. It follows from Eq. (8.26) that the Debye lengths for the two electrolytes in question are

$$\lambda_D(\text{NaCl},\ 10^{-1}\ \text{M}) = 1\ \text{nm} \ll h, \tag{17.9a}$$

$$\lambda_D(\text{water},\ 10^{-7}\ \text{M}) = 1\ \mu\text{m} > h. \tag{17.9b}$$

This, of course, just shows that the two electrolytes were carefully chosen to obtain the two extreme cases of Debye lengths either much smaller or much bigger than the channel heights. For simplicity, we apply the Debye–Hückel approximation in the analysis.

Even though no electrodes with applied voltages are attached in the capillary-filling experiments, electro-osmosis might come into play due to the charge convection currents I_{eo}^{conv} and I_{p}^{conv}, introduced and analyzed in Section 9.2. As the position $L(t)$ of the meniscus propagate into the nanochannel driven by the Young–Laplace pressure Δp_{surf}, the Poiseuille-like flow sets up a non-zero charge convection current, $I_{p}^{conv} \neq 0$, given by Eq. (9.33). However, unless opposed by countercurrents, such a convection current would result in a gradual charging of the nanochannel, which in the long run would lead to unrealistic charging energies. Consequently, in a lowest-order approximation the total electric current I through a given cross-section situated at $x \ll L(t)$ must vanish,

$$I = I_{p}^{conv} + I_{eo}^{conv} + I_{eo}^{cond} \equiv 0. \tag{17.10}$$

The counterflowing electro-osmotic current can be established through a small charging of the region near the meniscus, which leads to the existence of an electric field E that drives the EO flow. The magnitude of E is found by combining Eq. (17.10) with the explicit expressions for the conduction and convection currents given by Eqs. (9.22) and (9.33),

$$\left[1 + \alpha\, g(s_o)\right] wh(\sigma_{ion}^{+} + \sigma_{ion}^{-})E = f(s_o)\, wh \frac{\epsilon\zeta}{\eta} \frac{\Delta p}{L}, \tag{17.11}$$

where

$$s_o \equiv \frac{h}{2\lambda_D}, \tag{17.12a}$$

$$\alpha \equiv \frac{\epsilon^2\zeta^2}{2\lambda_D^2(\sigma_{ion}^{+} + \sigma_{ion}^{-})\eta}, \tag{17.12b}$$

$$f(s_o) \equiv \left[1 - \frac{1}{s_o}\tanh(s_o)\right], \tag{17.12c}$$

$$g(s_o) \equiv \frac{1}{s_o}\tanh(s_o) - \operatorname{sech}^2(s_o). \tag{17.12d}$$

These expressions lead to a determination of the magnitude v_{eo} of the EO flow necessary to guarantee a zero electric current

$$v_{eo} \equiv \frac{\epsilon\zeta}{\eta} E = \frac{\alpha f(s_o)}{1 + \alpha g(s_o)} \frac{2\lambda_D^2}{\eta} \frac{\Delta p}{L}. \tag{17.13}$$

Finally, by subtracting the counterflowing EO flow rate $Q_{eo} = wh\, v_{eo}\, f(s_o)$, given by Eq. (9.16), from the advancing Poiseuille flow $Q_p = wh^3 \Delta p_{surf}/(12\eta L)$, given by Eq. (7.34), we obtain an estimate of the total flow rate Q,

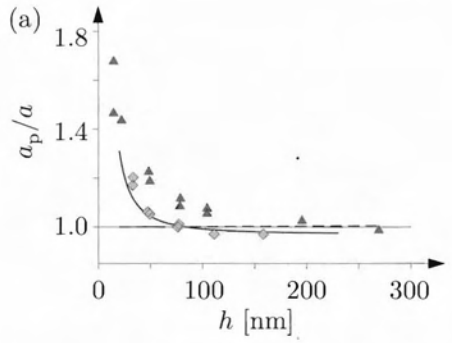

Fig. 17.5 (a) Calculated slope ratio $a_p/a = Q_p/Q$ as a function of channel height h obtained from Eq. (17.15) for 10^{-7} M water (dashed line) using $\zeta = 100$ mV and for 0.1 M NaCl (full line) using $\zeta = 250$ mV and a downshift of the base line with a factor of 0.97. The data from Fig. 17.4(b) are also shown: NaCl (light gray diamonds) and water (dark gray triangles).

$$Q = Q_p - Q_{eo} = \frac{wh^3}{12\eta}\frac{\Delta p}{L} - \frac{\alpha f^2(s_o)}{1+\alpha g(s_o)}\frac{2wh\lambda_D^2}{\eta}\frac{\Delta p}{L}$$
$$= Q_p\left[1 - \frac{6\alpha f^2(s_o)}{s_o^2\left[1+\alpha\, g(s_o)\right]}\right]. \tag{17.14}$$

Returning to Eq. (17.8), we can now use Eq. (17.14) to derive an expression for the expected deviation of the slope a from pure Poiseuille flow slope a_p,

$$\frac{a_p}{a} = \frac{Q_p}{Q} = \left[1 - \frac{6\alpha f^2(s_o)}{s_o^2\left[1+\alpha\, g(s_o)\right]}\right]^{-1}. \tag{17.15}$$

Let us first focus on the NaCl electrolyte with a Debye length $\lambda_D = 1$ nm much smaller than the channel height h. Since 30 nm $< h <$ 300 nm the variable s_o lies in the range $15 < s_o < 150$, and the slope ratio $a_p/a = Q_p/Q$ from Eq. (17.15) is approximately given by

$$\frac{a_p}{a} = \frac{Q_p}{Q} \approx \left[1 - \frac{6\alpha}{s_o^2}\right]^{-1}, \quad \text{for } s_o \gg 1. \tag{17.16}$$

It is clearly seen that the theory predicts an increase in the deviation of the expected slope from unity. In Fig. 17.5 is shown a theoretical fit based on the full equation (17.15) with parameters corresponding to 0.1 M NaCl to the data. The agreement is fair, but actually the theory outlined here cannot explain the observed phenomena. This becomes clear when turning to the case of 10^{-7} M water, where the large Debye length $\lambda_D = 1$ μm is larger than the channel height h. The variable s_o now lies in the range $0.01 < s_o < 0.15$, and in this limit a Taylor expansion of a_p/a yields

$$\frac{a_p}{a} = \frac{Q_p}{Q} \approx 1 + \frac{2}{3}\alpha\, s_o^2, \quad \text{for } s_o \ll 1. \tag{17.17}$$

This behavior of the slope ratio is completely wrong, since it is decreasing from values above unity towards unity, as the channel height is decreased. Inserting the parameter values for

pure water we obtain $Q_p/Q \approx 1 + 0.27\, s_o^2$, which increases from 1.000 at $s_o = 0.01$ to 1.006 at $s_o = 0.15$.

17.3 Squeeze flow in nanoimprint lithography

To fabricate nanofluidic channels one may choose to use the so-called nanoimprint lithography (NIL) process. Since this process itself utilizes nanofluidics, namely squeeze flow in liquid films with thicknesses of the order 100 nm, we will briefly study NIL in this section. NIL is a nanopatterning method, which combines nanometer-scale resolution with high throughput fabrication. A hard stamp containing the nanopattern is pressed into a thin polymer film deposited on a hard substrate. At sufficiently high temperature (above the glass-transition temperature T_g) the polymer melts and becomes a viscous liquid. Upon imprinting, as sketched in Fig. 17.6, the polymer therefore flows away from the regions beneath the protrusions of the stamp and into the cavities of the stamp. This flow process can be characterized as a nanofluidic squeeze flow in the polymer film, and in the following we analyze it assuming a simple model of the system.

We model the region below a given protrusion in the stamp as a parallel-plate system similar to the Couette flow system of Fig. 3.3, but now, as sketched in Fig. 17.7, moving the top plate downward antiparallel to the vertical z axis instead of parallel to the horizontal x axis. In squeeze flow, contrary to Couette flow, the height h of the liquid film between the bottom and top plates becomes a function $h(t)$ of time. We shall calculate how long it takes to squeeze the liquid film from some initial thickness h_0 to some final thickness h_f. This time is important as it sets the time scale for the NIL fabrication process. The stamp has the length $2L$ in the x direction and the width w in the y direction, so the polymer film fills the region $-L < x < L$ and $0 < y < w$.

To facilitate the calculation we make the following simplifying assumptions. The given, applied imprinting force F_{imp} on the stamp is constant in time, and for a sufficiently thin film the squeeze flow is so slow that in analogy with the capillary pump flow in Section 7.4.1 it can be regarded as quasi-steady. The validity of this fundamental assumption will be

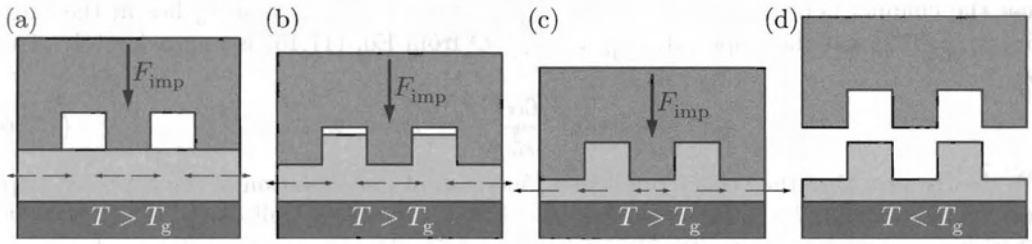

Fig. 17.6 The basic principle of nanoimprint lithography (NIL). (a) Initial phase: under the action of a constant force F_{imp}, the hard stamp is pressed into the soft, thin polymer film, which is deposited on a hard substrate and heated to above its glass-transition temperature T_g. (b) Intermediate phase: by the imprinting force F_{imp} the polymer film is slowly squeezed away from the regions beneath the protrusions of the stamp into the cavities or to the sides of the stamp. (c) Final phase: After complete filling of the cavities the polymer can only flow towards the sides of the stamp. (d) Demolding phase: the temperature is decreased below T_g, the polymer solidifies and the stamp is removed leaving behind the nanopattern from the stamp in the polymer film. Functional devices can be fabricated by further processing of the film.

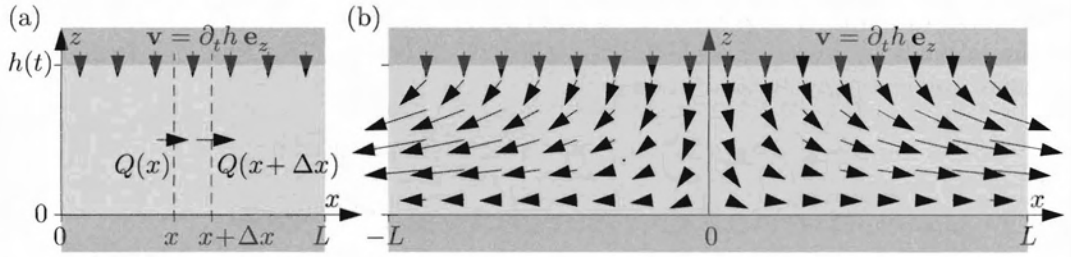

Fig. 17.7 Squeeze flow between parallel plates. (a) Conservation of mass for the slab of length Δx, width w (in the y direction), and height $h(t)$ leads to $Q(x+\Delta x) = Q(x) + \partial_t h\, w\Delta x$. (b) The velocity field Eq. (17.24), where it should be noted how the vertical component v_x increases as a function of horizontal distance x to the center of the channel at $x = 0$.

checked at the end of the calculation. If we, furthermore, consider $w \gg h(t)$ we can safely neglect edge effects from the edges at $y = 0$ and $y = w$, so at any given instant in time, where the film thickness is $h(t)$ and the speed of the stamp is $\partial_t h \equiv u_0$, the velocity field $\mathbf{v}$ must fulfill

$$\mathbf{v} = v_x(x,z)\,\mathbf{e}_x + v_z(x,z)\,\mathbf{e}_z, \text{ (quasi-steady 2D)}, \tag{17.18a}$$

$$\mathbf{v}(x,0) = \mathbf{0}, \qquad \text{(no-slip at fixed bottom plate)}, \tag{17.18b}$$

$$\mathbf{v}\big(x,h(t)\big) = \partial_t h\,\mathbf{e}_z \equiv -u_0\mathbf{e}_z, \qquad \text{(no-slip at moving top plate)}. \tag{17.18c}$$

The rheological properties of polymers are complex, but we shall nevertheless assume that the polymer film can be described adequately as an incompressible liquid with a constant viscosity η. This assumption can be justified given the very low Reynolds number and the constant temperature in the squeeze nanoflow. Finally, given the large imprinting pressure F_{imp} that typically is applied in NIL processes we neglect the influence of gravity. The governing equations for the squeeze nanoflow are thus the Stokes equation and the continuity equation,

$$\eta\big(\partial_x^2 + \partial_z^2\big)v_x(x,z) = \partial_x p(x,z), \tag{17.19a}$$

$$\eta\big(\partial_x^2 + \partial_z^2\big)v_z(x,z) = \partial_z p(x,z), \tag{17.19b}$$

$$\partial_x v_x + \partial_z v_z = 0. \tag{17.19c}$$

Given the quasi-steady flow we expect a Poiseuille-like flow profile along the x direction. The flow rate $Q(x)$ at a specific cross-section x can be determined by using the continuity equation on the slab of length Δx, width w, and height $h(t)$ as sketched in Fig. 17.7(a). The outflow to the right is given by the sum of the inflow from the left and from the top (denoting $\partial_t h \equiv -u_0$) as

$$Q(x+\Delta x) = Q(x) + u_0 w\,\Delta x, \quad \text{or} \quad \partial_x Q(x) = u_0 w. \tag{17.20}$$

By symmetry, the flow rate must be zero at the center plane $x = 0$ of the channel, so the position-dependent flow rate is therefore found to be

$$Q(x) = u_0 w\, x. \tag{17.21}$$

Combining this with the assumption of a local Poiseuille flow (to be checked by the end of the calculation) between parallel plates of length Δx, leads to the following form of the pressure gradient along the x direction,

$$\partial_x p = \lim_{\Delta x \to 0} \frac{\Delta p}{\Delta x} = -\lim_{\Delta x \to 0} \frac{12\eta \Delta x Q(x)}{w h^3 \Delta x} = -\frac{12\eta u_0}{h^3}\, x. \tag{17.22}$$

The x component of the Stokes equation (17.19a) becomes

$$\eta\big(\partial_x^2 + \partial_z^2\big) v_x = \partial_x p = -\frac{12\eta u_0}{h^3}\, x, \tag{17.23}$$

with the following solution that satisfies the boundary conditions,

$$v_x(x,z) = \frac{6u_0}{h^3}\, z(h-z)\, x. \tag{17.24a}$$

From this expression for $v_x(x,z)$ and the continuity equation $\partial_z v_z = -\partial_x v_x$, Eq. (17.19c), the z-component of the velocity is easily found by integration to be

$$v_z(x,z) = \frac{u_0}{h^3}\, z^2(2z-3h). \tag{17.24b}$$

We see that in agreement first-order perturbation theory, Eq. (14.6), the velocity in the z direction is smaller than the velocity in the x direction by a factor of $z/x \approx h(t)/L$.

Given the two velocity components we can calculate the streamlines of the flow by following the procedure outlined in Eq. (14.24). Each streamline of the form $\big(x(z), z\big)$ obeys the differential equation

$$\frac{\mathrm{d}z}{\mathrm{d}x} = \frac{v_z(x,z)}{v_x(x,z)} = \frac{z(2z-3h)}{6x(h-z)}. \tag{17.25}$$

By separation of the variables, see Exercise 17.5, we find the following explicit expression for the streamline through the point (x_0, h),

$$\mathbf{r}_{\{x_0,h\}}(z) = \begin{pmatrix} \dfrac{x_0 h^3}{z^2(3h-2z)} \\ z \end{pmatrix}. \tag{17.26}$$

A collection of streamlines is plotted in Fig. 17.8.

The non-trivial z-component of the velocity field implies a z-dependence in the pressure given by

$$\partial_z p = \eta\big(\partial_x^2 + \partial_z^2\big) v_z = \frac{6\eta u_0}{h^3}\,(z-h), \tag{17.27}$$

which together with $\partial_x p$ in Eq. (17.22) leads to the following pressure fulfilling the boundary condition $p(L,0) = p^*$,

$$p(x,z) = \frac{6\eta u_0}{h^3}\left[\big(L^2 - x^2\big) - z\big(h - \tfrac{1}{2}z\big) + p^*\right]. \tag{17.28}$$

We now have the solution for the velocity field $\mathbf{v}(x,z)$ and the pressure $p(x,z)$, which will allow us to calculate the imprinting time. However, before doing so we check if the

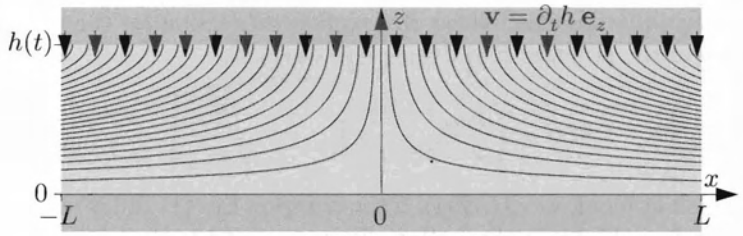

Fig. 17.8 The streamlines for squeeze flow between parallel plates, see Eq. (17.26) and Exercise 17.5. The downward velocity $\partial_t h$ of the top plate fulfills the criterion $\rho h|\partial_t h|/\eta \ll 1$ for quasi-steady motion.

solution in fact is in accordance with the assumptions. Most importantly, we have neglected the explicit time dependence $\rho\partial_t \mathbf{v}$ as well as the non-linear inertia $\rho(\mathbf{v}\cdot\boldsymbol{\nabla})\mathbf{v}$, so we now seek to explicitly state the criterion for this approximation to be valid, i.e. when these two terms are small compared to the only velocity-dependent term left in the equation, namely $\eta\nabla^2\mathbf{v}$.

The solutions for v_x and v_z are simple polynomials in x and z, so it is easy to obtain the following orders of magnitude estimates: $v_x \approx u_0 L/h$, $v_z \approx u_0$, $\partial_x \approx 1/L$, and $\partial_z \approx 1/h$, which for the inertial terms leads to $\rho(\mathbf{v}\cdot\boldsymbol{\nabla})v_i \approx (\rho u_0/h)v_i$, where $i = x, z$, while the viscous terms become $\eta\nabla^2 v_i \approx (\eta/h^2)v_i$. Since the time dependence in the solution only appears through $h(t)$ we can estimate the order of magnitude of the acceleration term as $\rho\partial_t v_i = \rho(\partial_t h)\partial_h v_i \approx (\rho u_0/h)v_i$, i.e. the same as the inertial term. The criterion for the validity of the approximative solution is that the Reynolds number-like quantity $\rho h u_0/\eta$ is much smaller than unity,

$$\frac{|\rho\partial_t v_i|}{|\eta\nabla^2 v_i|}, \frac{|\rho(\mathbf{v}\cdot\boldsymbol{\nabla})v_i|}{|\eta\nabla^2 v_i|} \approx \frac{(\rho u_0/h)v_i}{(\eta/h^2)v_i} = \frac{\rho h u_0}{\eta} = \frac{\rho h|\partial_t h|}{\eta} = \frac{\rho|\partial_t(h^2)|}{2\eta} \ll 1. \tag{17.29}$$

The slower the motion of the stamp the better is the approximative solution.

The imprinting time τ_{imp} is defined as the time it takes to squeeze the polymer film from a given initial thickness $h(0) = h_0$ to a given final thickness $h(\tau_{\text{imp}}) = h_{\text{f}}$. It is calculated by considering the average imprinting pressure $p_{\text{imp}} = \langle p(x,z) - p^*\rangle$ derived from Eq. (17.28). If we disregard the small contribution from the z-dependent part of the pressure, which is suppressed by a factor of h^2/L^2 we obtain

$$p_{\text{imp}} = \frac{1}{2L}\int_{-L}^{L} \mathrm{d}x \left[p(x,0) - p^*\right] = \frac{4\eta u_0 L^2}{h^3} = -\frac{4\eta L^2 \partial_t h}{h^3}. \tag{17.30}$$

The imprinting pressure can be expressed in terms of the constant imprinting force acting on the area $(2L)w$ of the top plate as, $p_{\text{imp}} = F_{\text{imp}}/(2Lw)$, and upon separation of the variables t and h in Eq. (17.30) we find

$$\tau_{\text{imp}} = \int_0^{\tau_{\text{imp}}} \mathrm{d}t = -\frac{4\eta L^2}{p_{\text{imp}}}\int_{h_0}^{h_{\text{f}}} \frac{\mathrm{d}h}{h^3} = \frac{2\eta L^2}{p_{\text{imp}}}\left[\frac{1}{h_{\text{f}}^2} - \frac{1}{h_0^2}\right] = \frac{\eta(2L)^3 w}{2F_{\text{imp}}}\left[\frac{1}{h_{\text{f}}^2} - \frac{1}{h_0^2}\right]. \tag{17.31}$$

In the literature, this expression is known as the Stefan equation.

From the Stefan equation also follows the explicit expression for the time dependence of the thickness $h(t)$ of the polymer film during squeeze flow,

$$h(t) = \left(\frac{p_{\text{imp}} t}{2\eta L^2} + \frac{1}{h_0^2} \right)^{-\frac{1}{2}} \approx \sqrt{\frac{2\eta L^2}{p_{\text{imp}} t}}. \tag{17.32}$$

With this expression at hand, we can check if the criterion Eq. (17.29) is fulfilled. By squaring and differentiating Eq. (17.32) we find after elimination of t by h that

$$\frac{\mathrm{d}h^2}{\mathrm{d}t} = \frac{p_{\text{imp}} h^4}{2\eta L^2}. \tag{17.33}$$

Inserting appropriate parameter values for NIL by hot embossing in the polymer PMMA, for which $p_{\text{imp}} \approx 10^6$ Pa, $\eta \approx 10^5$ Pa s, $\rho \approx 2 \times 10^3$ kg m^{-3}, and taking the typical length scales $h \approx 10^{-6}$ m and $L \approx 10^{-5}$ m we find

$$\frac{\rho |\partial_t (h^2)|}{2\eta} \approx 10^{-15} \ll 1. \tag{17.34}$$

One can safely conclude that the solution is accurate. For the same parameters, as studied in Exercise 17.6 the Stefan equation leads to imprinting times of the order

$$\tau_{\text{imp}} \approx 10^2 \text{ s}, \quad (1 \text{ µm thick PMMA film at } 10^6 \text{ Pa}). \tag{17.35}$$

17.4 Nanofluidics and molecular dynamics

In Section 1.3.2 the continuum description was introduced by applying the concept of averaging over molecular quantities in mesoscopic volumes. It is therefore of importance to verify and study the applicability of this fundamental description by direct simulation of liquids on the molecular level. One such method is the widely used molecular dynamics (MD) method. This method is well suited for simulating liquids in volumes of linear size less than 100 nm and for short time intervals less than 5 ns. Although severely restricted to this small space-time domain, the MD method nevertheless allows for first-principles calculations of liquid properties and behavior, and it might also provide important insight under conditions, where the continuum description fails, e.g. due to very strong spatial confinements or very high shear stresses.

The typical MD simulation comprises three main steps: (*i*) Setup of the geometry and the initial conditions, (*ii*) specification of the intermolecular interaction potential, and (*iii*) time integration of the molecular equation of motion.

In step (*i*) a calculational grid is defined to match the geometry of the given problem. A set of molecules i is introduced with positions $\mathbf{r}_i$ on randomly selected grid points, and each molecule is assigned with a random energy ε_i in accordance with the Maxwell distribution $f(\varepsilon_i) \propto \exp(-\varepsilon_i / k_{\text{B}} T)$. In step (*ii*) a pair-interaction potential $V(r_{ij})$ is introduced for a pair of molecules positioned at $\mathbf{r}_i$ and $\mathbf{r}_j$ and with $r_{ij} \equiv |\mathbf{r}_i - \mathbf{r}_j|$. Often, the pair-potential is some variant of the Lennard-Jones potential V_{LJ} introduced in Section 1.3.1 and Exercise 1.2,

$$V_{\text{LJ}}(r_{ij}) = 4\varepsilon \left[\left(\frac{\sigma}{r_{ij}} \right)^{12} - \left(\frac{\sigma}{r_{ij}} \right)^{6} \right]. \tag{17.36}$$

Finally, in step (*iii*) a time integration is performed of the molecular equation of motion, which typically is simply Newton's second law. For molecules of mass m moving in contact

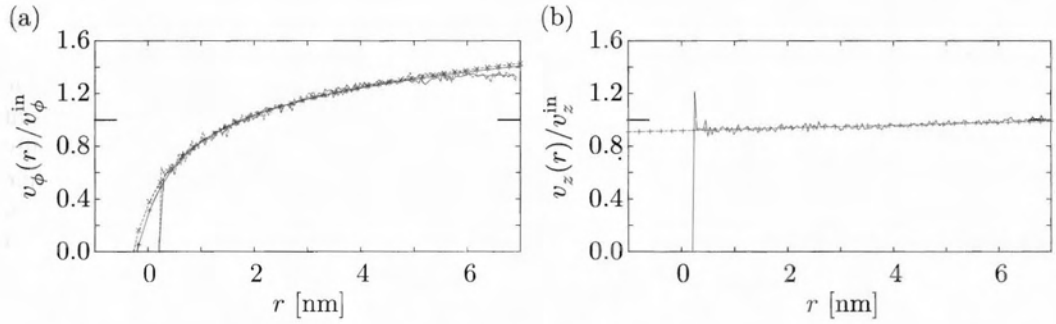

Fig. 17.9 Molecular dynamics calculation of the slip length for water flowing past a carbon nanotube of diameter 2.5 nm. (a) The azimuthal velocity component $v_\phi(r)$ normalized by the inflow value as a function of the distance r from the surface of the carbon nanotube. The slip length is found to be $\lambda_s(v_\phi) = 0.40$ nm. (b) The axial velocity component $v_z(r)$ normalized by the inflow value as a function of the distance r from the surface of the carbon nanotube. The slip length is found to be $\lambda_s(v_z) = 88$ nm. Figures reprinted by permission from J. H. Walther *et al.*, Phys. Rev. E **69**, 062201 (2004). Copyright (2004) by the American Physical Society.

with a dissipative thermal reservoir having the equilibration time τ the equation of motion could be of the form

$$m\,\frac{\mathrm{d}^2\mathbf{r}_i}{\mathrm{d}t^2} = \sum_{j\neq i} \partial_{\mathbf{r}_i} V(r_{ij}) - \frac{m}{\tau}\,\frac{\mathrm{d}\mathbf{r}_i}{\mathrm{d}t}. \tag{17.37}$$

With modern computers it is possible to compute the behavior of up to 10^6 molecules in the previously mentioned small space-time domain. Using advanced time integration methods and allowing for suitable equilibration time period, typically 10 to 100 τ, averages of the molecular properties can be obtained. The calculation domain is divided into a number of bins α each situated around a position $\mathbf{x}_\alpha$, and, e.g. the Eulerian velocity $\mathbf{v}(\mathbf{x}_\alpha)$ is obtained as the time average of the velocity of the molecules of mass m_i inside the bin,

$$\mathbf{v}(\mathbf{x}_\alpha) \equiv \frac{\left\langle \sum_{i\in\alpha} m_i \frac{\mathrm{d}\mathbf{r}_i}{\mathrm{d}t} \right\rangle_t}{\left\langle \sum_{i\in\alpha} m_i \right\rangle_t}. \tag{17.38}$$

The field of molecular dynamics is highly developed and many tricks and methods have been introduced over the years. The above introduction is very rudimentary and the reader interested in the MD method is referred to textbook by Allen and Tildesley (1994) or the review paper by Koplik and Banavar (1995).

We end this short section on molecular dynamics by a brief presentation of the results obtained by the group of Koumoutsakos at ETH Zürich, see Walther *et al.* (2004) regarding calculations of the slip length λ_s introduced in Section 17.1. In the center of a flat parallelepiped of size $L_x = 16.4$ nm, $L_y = 16.4$ nm, and $L_z = 2.1$ nm, a carbon nanotube of diameter 2.5 nm was placed parallel to the z axes. The nanotube consisting of 640 atoms was surrounded by 1.8×10^4 water molecules. To ensure that the average velocity is much larger than the statistical spread, the flow speed was set to be of the order 100 m/s $< 0.15 c_a$. Although this value is much higher than the typical flow speed in microfluidics, it is not

so high as to introduce either non-linear or acoustic effects, so the obtained results can be down-scaled.

The flow direction was chosen to have a non-trivial angle of 17° with respect to the carbon nanotube axis, and thereby there was both an azimuthal component v_ϕ and an axial component v_z of the velocity. These two velocity components were sampled statistically by dividing the computational domain into 6 azimuthal bins and 200 radial bins, while the density was sampled using 1600 radial bins. The result of the calculation is shown in Fig. 17.9, where it is seen that the calculated slip length for the strongly curved azimuthal velocity component is very short, while it is much longer for the axial velocity component,

$$\lambda_s(v_\phi) = 0.40 \text{ nm}, \tag{17.39a}$$

$$\lambda_s(v_z) = 88 \text{ nm}. \tag{17.39b}$$

Walther *et al.* conjecture that the slip length is related to the presence of a stagnation point of the flow, and hence to the particular geometry. It is interesting to note that the long slip length calculated for the water-carbon interface along the flat axial direction is comparable to the experimental result 50 nm ± 50 nm measured on the flat water-glass interface discussed in Section 17.1. The question about the value of the slip length remains open both experimentally as well as theoretically. It is one of the exciting research topics in nanofludics.

17.5 Exercises

Exercise 17.1

Hydraulic resistance for a non-zero slip length in a flat channel

Consider a pressure-driven flow in an infinite parallel-plate channel of height h given a Navier boundary condition with a non-zero slip length λ_s on both bottom and top plates.

(a) Derive the expression for the velocity profile $v_x(z)$. Hint: due to symmetry the problem is easier solved when placing the bottom plate at $\tilde{z} = -h/2$ and the top plate at $\tilde{z} = h/2$.

(b) Derive the expression for the hydraulic resistance $R_{\text{hyd}}(\lambda_s)$ based on the velocity profile derived above. Express the result as $R_{\text{hyd}}(\lambda_s) = f(\lambda_s)\, R_{\text{hyd}}(0)$.

(c) The experimental results in Fig. 17.2(b) points toward a slip length $\lambda_s = 50$ nm. Calculate the relative change in the hydraulic resistance when changing λ_s from 0 nm to 50 nm in the case of microchannels with height $h = 10$ µm and 1 µm.

Exercise 17.2

Hydraulic resistance for a non-zero slip length in a circular channel

Consider a pressure-driven flow in a straight channel of length L with a circular cross-section of radius a given the Navier boundary condition with a non-zero slip length λ_s at the channel wall.

(a) Derive the expressions for the slip length dependent velocity profile $v_x(z)$ and for the hydraulic resistance $R_{\text{hyd}}(\lambda_s)$.

(b) Calculate the relative change in the hydraulic resistance when changing λ_s from 0 nm to 50 nm for the two values of the radius $a = 5$ µm and 0.5 µm.

Exercise 17.3
Brownian motion of tracer particles
In the PIV measurements of the slip length tracer particles of radius $a = 50$ nm were employed.

(a) Calculate the diffusion constant D of the tracer particles in deionized water at room temperature.

(b) The PIV measurements involved a recording region of height $\Delta z = 500$ nm and a time interval $\tau = 20$ ms between each pair of pictures on which the PIV analysis is based. Discuss the likelihood of tracer particles blurring the PIV signal by diffusing in or out of the recording region in the time interval τ between the two pictures in a pair of PIV pictures.

Exercise 17.4
The Debye length of pure water and 0.1 M NaCl
The pH value of pure water is 7, which by definition means that the proton concentration is $c = 10^{-7}$ M. Calculate the Debye length λ_D for pure water and for 0.1 M NaCl used in the experiments of the capillary filling of nanochannels, see Section 17.2.

Exercise 17.5
Streamlines of the quasi-steady squeeze flow
Calculate the streamlines for the squeeze flow in the quasi-steady limit given by the velocity field $\big(v_x(x,z), v_z(x,z)\big)$ in Eq. (17.24). Hint: separate the variables in the defining differential equation $\mathrm{d}x/v_x = \mathrm{d}z/v_z$ and find x as a function of z.

Exercise 17.6
Nanoimprint lithography time
Consider a nanoimprint stamp covering the area 1 mm $\times$ 1 mm consisting of a number of parallel rectangular cavities of length $L_c = 30$ µm in the x direction, width $w = 1$ mm in the y direction, and height $h_c = 200$ nm in the z direction, and separated by protrusions of length $2L = 20$ µm in the x direction, see Fig. 17.6. The incompressible polymer film has a viscosity of $\eta = 10^5$ Pa s and an initial thickness of $h_0 = 300$ nm. The nanoimprint pressure is constant and given by $p_{\mathrm{imp}} = 5$ MPa.

(a) Calculate the final film thickness h_f defined as the thickness underneath the protrusions exactly at the moment where the cavities are filled with polymer. Hint: use the fact that the polymer can be treated as an incompressible liquid.

(b) Use the Stefan equation to estimate the time τ_{imp} it takes to squeeze the polymer film from the initial thickness h_0 to the final thickness h_f.

(c) Estimate the ratio ᚠ between the imprint speed $\partial_t h$ just after and just before the final film thickness has been reached[1]. Hint: although denoted the final thickness, the polymer film continues to be squeezed after the cavities are filled at the thickness h_f, however, now the polymer has to flow all the way to the edges of the stamp.

17.6 Solutions

Solution 17.1
Hydraulic resistance for a non-zero slip length in a flat channel
The starting point is the Navier–Stokes equation (3.20a).

[1]Here, at the end of the book there is a shortage of latin and greek letters for naming the variables, hence this use of the first letter ᚠ (fehu) in the futhark runic alphabet of my ancestors, the vikings.

(a) With the Navier boundary condition applied at $\tilde{z} = \pm h/2$, the solution to the Navier–Stokes equation has the symmetric form

$$v_x(\tilde{z}) = \frac{\Delta p}{2\eta L}\left(z_0^2 - \tilde{z}^2\right). \tag{17.40}$$

Application of the Navier boundary condition $\partial_{\tilde{z}} v_x = \lambda_s v_x$ at $\tilde{z} = -h/2$ leads to the condition $\lambda_s h = z_0^2 - (h/2)^2$ or

$$z_0 = \pm\frac{h}{2}\sqrt{1 + 4\frac{\lambda_s}{h}}, \tag{17.41}$$

which upon insertion into Eq. (17.40) yields Eq. (17.4).

(b) The flow rate is found by integration of Eq. (17.40),

$$Q = 2\frac{\Delta p\, w}{2\eta L}\int_0^{\frac{h}{2}} \mathrm{d}\tilde{z}\left(z_0^2 - \tilde{z}^2\right) = \frac{\Delta p\, w}{\eta L}\left[z_0^2\frac{h}{2} - \frac{1}{3}\left(\frac{h}{2}\right)^3\right] = \frac{\Delta p\, w h^3}{12\eta L}\left[1 + 6\frac{\lambda_s}{h}\right]. \tag{17.42}$$

Since $R_{\mathrm{hyd}} = \Delta p/Q$ we find the hydraulic resistance to be given by Eq. (17.5).

(c) For $h = 10$ μm we find $R_{\mathrm{hyd}}(\lambda_s) = R_{\mathrm{hyd}}(0)/(1+6\times 0.05/10) = 0.97 R_{\mathrm{hyd}}(0)$. Similarly, for $h = 1$ μm we find $R_{\mathrm{hyd}}(\lambda_s) = R_{\mathrm{hyd}}(0)/(1 + 6 \times 0.05/1) = 0.77\, R_{\mathrm{hyd}}(0)$.

Solution 17.2

Hydraulic resistance for a non-zero slip length in a circular channel

The starting point is the usual Poiseuille flow in a channel with circular cross-section presented in Section 3.4.4.

(a) Since only the boundary condition has changed, the velocity field as a form similar to Eq. (3.42a)

$$v_x(r) = \frac{\Delta p}{4\eta L}\left(r_0^2 - r^2\right), \tag{17.43}$$

where the radius a has been substituted with an unknown constant r_0 to be determined. We note that the Navier boundary condition Eq. (17.2b) becomes $v_x(a)\,\mathbf{e}_x = -\lambda_s\left[\partial_r v_x(a)\right]\mathbf{e}_x$, which leads to the condition

$$r_0 = a\sqrt{1 + 2\frac{\lambda_s}{a}}, \tag{17.44}$$

which upon insertion into Eq. (17.43) yields

$$v_x(r) = \frac{\Delta p}{4\eta L}\left[\left(1 + 2\frac{\lambda_s}{a}\right)a^2 - r^2\right]. \tag{17.45}$$

The flow rate is found as $Q = 2\pi\int_0^a \mathrm{d}r\, r v_x(r)$, which straightforwardly leads to the hydraulic resistance,

$$R_{\mathrm{hyd}}(\lambda_s) = \frac{Q(\lambda_s)}{\Delta p} = \frac{\pi a^4 \Delta p}{8\eta L}\frac{1}{1 + 4\frac{\lambda_s}{a}} = \frac{R_{\mathrm{hyd}}(0)}{1 + 4\frac{\lambda_s}{a}}. \tag{17.46}$$

(b) For $a = 5$ μm we find $R_{\mathrm{hyd}}(\lambda_s) = R_{\mathrm{hyd}}(0)/(1 + 4 \times 0.05/5) = 0.96\, R_{\mathrm{hyd}}(0)$. Similarly, for $a = 0.5$ μm we find $R_{\mathrm{hyd}}(\lambda_s) = R_{\mathrm{hyd}}(0)/(1 + 4 \times 0.05/0.5) = 0.71\, R_{\mathrm{hyd}}(0)$. We note that when introducing a slip length λ_s, the hydraulic resistance decreases relatively more for a circular channel compared to a flat channel of height $h = 2a$. This is expected, since the lack of side walls in the flat channel implies no lowering of the resistance at the side regions of the channel upon introducing a non-zero slip length.

Solution 17.3
Brownian motion of tracer particles
The diffusion constant D is found from the Einstein relation Eq. (6.49).

(a) For room temperature $T = 300$ K, particle radius $a = 50$ nm, and viscosity $\eta = 1$ mPa s we find

$$D = \frac{k_B T}{6\pi a \eta} = 4.4 \times 10^{-12} \mathrm{m}^2/\mathrm{s}. \tag{17.47}$$

(b) Tracer particles will leave/enter the recording volume if the distance ℓ they diffuse in the time interval $\tau = 20$ ms is larger than the thickness $\Delta z = 500$ nm of the recording volume. Basic diffusion theory, see Eq. (5.8), gives $\ell \approx \sqrt{D\tau} = 300$ nm. This distance is smaller than but comparable to Δz, so these tracer particles are the smallest possible to use given the PIV requirements. The majority of tracer particles are likely to stay in the recording region, during the recording of one pair of PIV pictures. Smaller tracer particles would diffuse in and out of the recording region thus being a source of significant noise in the measurements.

Solution 17.4
The Debye length of pure water and 0.1 M NaCl
In Eq. (8.27) we found $\lambda_D(1 \text{ mM}) = 10$ nm. Since, according to Eq. (8.26) we have $\lambda_D \propto 1/\sqrt{c}$, we readily obtain $\lambda_D(10^{-7} \text{ M}) = 100\, \lambda_D(1 \text{ mM}) = 1$ μm and $\lambda_D(100 \text{ mM}) = 0.1\, \lambda_D(1 \text{ mM}) = 1$ nm.

Solution 17.5
Streamlines of the quasi-steady squeeze flow
From the definition of streamlines, $\mathrm{d}x/v_x = \mathrm{d}z/v_z$, and the velocity field in Eq. (17.24), we easily establish the differential equation given in Eq. (17.25). By separation of the variables it is transformed into

$$\frac{6(h-z)}{z(2z-3h)}\,\mathrm{d}z = \frac{1}{x}\,\mathrm{d}x. \tag{17.48}$$

We note that $6(h-z)/[z(2z-3h)] = 2/(3h-2z) - 2/z$, and integration leads to the logarithms $-\log(3h-2z) - 2\log z = \log x - \log A$, where A is an integration constant. Taking the exponential of both sides gives the result

$$x(z) = \frac{x_0 h^3}{z^2(3h-2z)}, \tag{17.49}$$

where the integration constant has be chosen so that the streamline passes through the point (x_0, h) on the top plate. This expression is the basis for Fig. 17.8.

Solution 17.6
Nanoimprint lithography time
When the stamp has sunk the vertical distance Δh each protrusion has displaced the volume $\Delta h(2L)w$, while each cavity has received this amount of polymer as well as the volume $\Delta h L_c w$ of the polymer residing underneath the sinking cavity.

(a) The final film thickness is reached when the cavity volume equals the sum of these two polymer volumes, $h_c L_c w = \Delta h(L_c + 2L)w$. Since $\Delta h = h_0 - h_f$ we get

$$h_f = h_0 - \frac{L_c}{L_c + 2L}\, h_c = 180 \text{ nm}. \tag{17.50}$$

(b) Given the result above we can now apply the Stefan equation with the parameter values $\eta = 10^5$ Pa s, $L = 10$ µm, $p_{\text{imp}} = 5$ MPa, $h_0 = 300$ nm, and $h_{\text{f}} = 180$ nm,

$$\tau_{\text{imp}} = \int_0^{\tau_{\text{imp}}} \mathrm{d}t = \frac{2\eta L^2}{p_{\text{imp}}} \left[\frac{1}{h_{\text{f}}^2} - \frac{1}{h_0^2} \right] = 80 \text{ s}. \tag{17.51}$$

(c) The imprint speed $\partial_t h$ can be found by differentiating Eq. (17.32) with respect to time, or more easily in this case, directly from Eq. (17.30)

$$\partial_t h(t) = -\frac{p_{\text{imp}} h^3}{4\eta L^2}. \tag{17.52}$$

The difference between the situation just before and just after the cavities have been filled lies solely in the interpretation of the length L. Before the complete filling L is to be taken as half the length of the protrusions, here $L = 10$ µm, since the polymer only has to flow from underneath one protrusion to the neighboring cavity. After complete filling the polymer has to flow all the way to the edges, i.e. L is now half the size of the stamp, here $L = 500$ µm. The imprint speed thus decreases abruptly by a factor of the order of $\text{f} = (10 \text{ µm}/500 \text{ µm})^2 = 4 \times 10^{-4}$ once the stamp cavities has been filled with polymer.